AUTOMATYKA • 2006 • Tom 10 • Zeszyt 3

Laurent Babout*

X-Ray Tomography Imaging: a Necessary Tool for Materials Science

1. Introduction

For many people, X-ray tomography, also known as CT (Computed Tomography) or CAT-scan (Computed Axial Tomography), is devoted for medical applications to visualize three-dimensional images of human body. The technique has been firstly commercialized in the 70's, and different types of generation have been developed (mainly linked with different acquisition procedures) in order to mainly improve the acquisition speed. However, CT scans are less popular than Magnetic Resonance Imaging (MRI) which normally provides a far better contrast resolution with similar spatial resolution, and above all, which is harmless to patient (X-ray radiation dose may increase the chance of malignancy, especially in a fetus). Nowadays, the number of applications of X-ray tomography in other field of research than in medicine is constantly increasing, such as in paleontology, archeology or in materials science. In the past 10 years, the technique has known a real breakthrough, with the development of worldwide synchrotron radiation tomography apparatus which can provide 3D images with a spatial resolution 100–200 times higher than conventional medical CT systems. The commercialization of industrial and laboratory based system with microscale resolution has also steeply increased and X-ray tomography system is becoming an inevitable imaging tool to be own by research institutes, in the same respect as well known secondary and transmission electron microscopes.

Nowadays, X-ray tomography can really compete with classical optical and electronic microscopy techniques because:

- the technique is non invasive and there is no need for sample preparation like polishing,
- very brittle sample can be easily handled,
- in situ mechanical test can be monitored on tomography stage,
- the spatial resolution is equivalent to optical microscope (up to 20× magnification),
- and, of course, three dimensional images are reconstructed.

* Department of Computer Engineering, Technical University of Łódź

This paper presents two examples with industrial implications to attest the state-of-the-art of the technique from two different types of apparatus mentioned above: synchrotron X-ray microtomography and laboratory X-ray CT. The respective examples deal with nuclear graphite and titanium alloy for aeroengine industry.

2. X-ray tomography: basic principle and set-ups

The general concept of X-ray tomography is an extension of classical X-ray radiography, and is based on the attenuation of the X-ray beam through the specimen. X-ray radiography provides only a projection of the sample volume on one single plane. X-ray tomography overcomes this disadvantage by combining the information from a series of many radiographs, each being recorded with different orientation of the sample in front of the detector. The variation of X-ray attenuation in the volume of the sample can be reconstructed by combining a sufficient number of radiographs with an appropriate algorithm, such as filtered back-projection (Feldkamp *et al.* 1984). The data is obtained in the form of a three-dimensional array of voxels (analogous to pixels in a two-dimensional digital image), for which the grey-level of each voxel describes the calculated X-ray attenuation at that position. Dedicated imaging software have been developed like Amira or VGStudiomax, with some of them in shareware such as ImageJ. The image processing toolbox in Matlab also offers some possibilities to deal with 3D images.

A tomographic scan requires an X-ray source, a rotation stage and an X-ray detector. This is usually a fluorescent detector which changes the X-rays into visible light, and a set of optic lenses that transfers the light to a CCD camera. Cone and parallel X-ray sources are commonly used. The term microtomography is sometimes used to refer to tomography with an image spatial resolution in the micron range, which can be achieved if the spot size is of the order of few microns, or via an adequate set of optics in the detector. The main drawback of the technique lies in the sample size limitation, which need to stand in the field of view of the camera. For instance, if a 1024^2 CCD chip is used with a 2 μm pixel size, the maximum sample size in the transversal cross section is ~2 mm.

The two examples presented in this article have been obtained separately on laboratory tomograph at the Materials Science Centre, University of Manchester (UK) and at the European Synchrotron Radiation Facility (ESRF, Grenoble, France), on the ID19 beam line. The first tomograph device (setup1 hereafter), shown in Figure 1 uses an X-ray fan beam with a maximum energy of 225 keV, a focal spot size of around 9 μm and a spot angle of 80°. The system is composed with two different detectors equipped with beryllium and aluminum foils adequate for low and high material density respectively. The main features of the second tomograph (setup 2 hereafter) are a spectrally and spatially homogeneous, highly coherent, high photon flux beam at the sample position, and a tunable photon energy in the range of 6–100 keV, with most of the experiments done in the range 10–35 keV(Boller 2005). A state-of-the-art detector, developed at the ESRF, allows radiographs to be acquired with a tunable spatial resolution in the range of 0.29–40 μm with a fast readout (20 Mpixel/s) and very low readout noise (25 e^-).

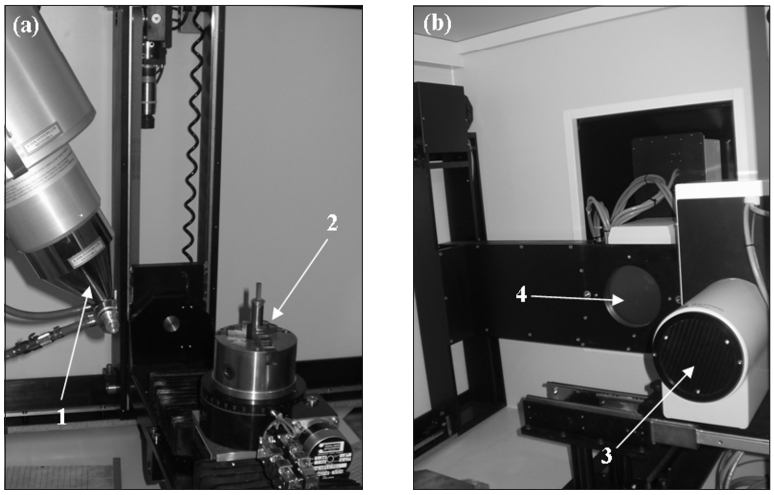

Fig. 1. X-ray tomograph "system1": a) view of X-ray fan beam source and rotation stage; b) view of two different detectors. 1 – X-ray source, 2 – rotation stage, 3 – beryllium foil detector, 4 – aluminum foil detector

Table 1 presents the different set-ups applied to the two examples presented in this paper. One can see the relative fast scan duration of both systems for the very high spatial resolution and number of radiographs used.

Table 1
Tomography parameters for setup 1 and 2. E – energy, R – resolution, t – exposure time, A – rotation step, Nr – number of radiographs, Nf – number of frame/radiograph, T – scan duration

		E(keV)	R(μm)	t(s)	A(°)	Nr	Nf	T(min)
Example1	Setup1	30	13	0.16	0.3	600	32	~50
Example2	Setup2	31	0.7	1.5	0.12	1500	1	~50

3. Experimental examples

3.1. Example 1: nuclear graphite

Graphite is a major component in gas-cooled reactor because it is a moderator for fast neutrons, has good thermal and mechanical properties. However, during servicing, oxidation at high temperature (i.e. 600–900ºC) are susceptible to generate microstructural changes in graphite, such as porosity development, which can lead to the damage, then potential failure of core component, which can have a major effect on the reactor functioning. There is then an important need in predicting the behavior of graphite, and the accuracy of the prediction is necessary linked with the understanding of the microstructure behavior. X-ray

tomography is then extremely adapted for the purpose of such study because the porosity network can be easily separated from the graphite during image segmentation and the voxels value in the 3D volume can be directly linked to local density (Babout *et al.* 2005; Babout *et al.* 2006). Example of such possibility is shown on Figure 2 which presents the microstructure before and after segmentation of a graphite sample before oxidation. Setup 1 was used for the tomography scans. Figure 2a clearly shows the typical porous microstructure of graphite present in the matrix phase (M) or within inclusions (I). The segmentation with a simple thresholding procedure is satisfying to select most of the porosity within the material. Only the smallest pores exhibiting less contrast with the graphite are not segmented (like MC type).

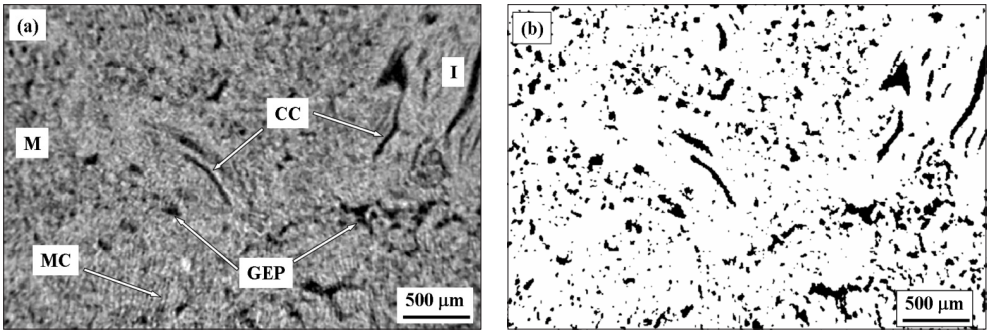

Fig. 2. X-ray tomography of graphite microstructure: a) grey level; b) after pore segmentation. M – matrix, I – inclusion, CC,GEP and MC are different types of porosity (Babout 2005)

Because graphite is only composed with one chemical element, namely carbon, it is possible to correlate the local attenuation in the original 3D volume with the real local density after step wedge calibration (Babout 2006). This is then very useful to quantify the variation of density within the material, especially after graphite has been subjected to thermal oxidation. An example of such quantification is shown in Figure 3. This quantification has been performed using a 3D-density mapping function written in Matlab. The function considers a cubical region containing an odd number of voxels on each dimension centered in turn on each voxel. The grey level value of the voxel is replaced by the average value of the including box (averaging volume). The boundary problem associated with the voxels that lie nearer to the edge of the volume than the half-width of the box, is solved by assuming that the volume edges are mirrors, so that each plane containing these voxels is duplicated beyond it. This "kernel" operation of neighborhood averaging, usually used in image treatment for noise reduction (Russ 1995), allows the block to be smoothed and reveals more clearly the average density fluctuation throughout the specimen. Naturally, the larger the averaging volume (box), the more homogeneous the density map. In the present case, a box size of 286 μm (i.e. 22 voxels) was found suitable to quantify density fluctuations (Babout 2006). An essentially uniform density across the virgin graphite sample is observed except around the large pores (located at the top of Fig. 3a). Apart from these large pores, most of the network of porosity has disappeared from the volume under the averaging ope-

ration, as their average equivalent diameter, i.e. 170 μm, is lower than the box size. Figure 3b shows the density map with the same kernel size for graphite sample thermally oxidized at 900°C. In contrast to the virgin state, a local microscale variation of density occurs in the thermally oxidized sample. The variation is due to the differing propensity for thermal oxidation of the matrix and the inclusions, which have average densities close to 1.0 and 1.6 g/cm^3 respectively. Figure 3b, compared with Figure 2a, reveals that the thermal oxidation process occurs preferentially in the matrix. This is mainly due to open porosity which works as a channel for carbon diffusion during thermal oxidation at 900°C. X-ray tomography imaging is the only technique which can perform the quantification of real density variation non-destructively and in three dimensions.

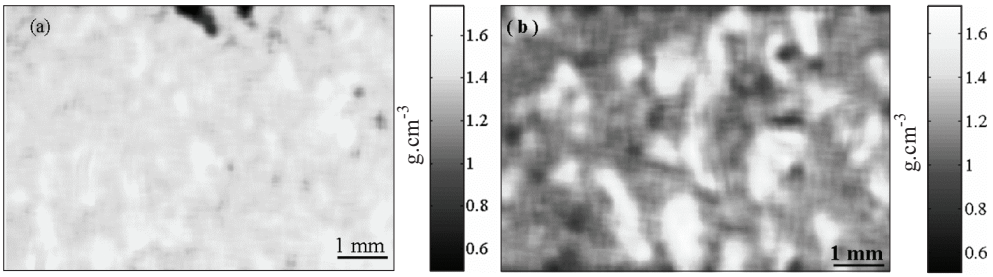

Fig. 3. Density maps of: a) virgin graphite; b) thermally oxidized graphite (weight loss of ~23%). Kernel box size: 286 μm

3.2. Example 2: titanium alloy

Titanium alloys find many applications in the aeroengine industry for their good tensile and fatigue strength properties at high temperature. They are often fabricated with a lamellar microstructure which comprises complicated 3D α lamellar colonies (α corresponds to hexagonal close-packed (hcp) crystal structure) embedded in large β grains (β corresponds to body centered cubic (bcc) crystal structure). Further details about this type of microstructure can be found in (Lutjering 1998). Observations of the interaction between the 3D fatigue crack and the (α+β) microstructure is one of the crucial steps to improve the prediction of the material lifetime using microstructure models. This type of crack tracking can be performed in situ by mounting a dedicated fatigue machine on the rotation stage of the tomography system in setup2.

The 3D images shown in Figure 4 present the comparison between the initial stage and one of two fatigued stages of a notched (α+β) titanium alloy sample. One can see that the lamellar microstructure can be satisfyingly observed, with a primary grain boundary (detail 2 in Fig. 4a) separating two grains clearly visualized. Some α lamellar colonies situated within β grain are also clearly distinguishable. A closer look shows that white fringes are situated between lamellae and along β grain boundary. Figure 4b also highlights the presence of cracks (cracks 1 and 2) initiated at a triangular-shape notch. A closer look of the cracks shows that they are surrounded by sharp white fringes. These fringes also complete the crack path in some places where no black line is visible. This type of image enhance-

ment which reveals the microstructure and some sub-resolution parts of the crack path using X-ray tomography is called edge or phase contrast (Cloetens *et al.* 1997). A necessary condition to generate such contrast is the spatial coherency of X-ray beam (see section 2). It is generated by the difference in refractive index between α and β phases or titanium and air, and it is amplified simply by increasing the sample – detector distance (100 mm to visualize the microstructure in titanium).

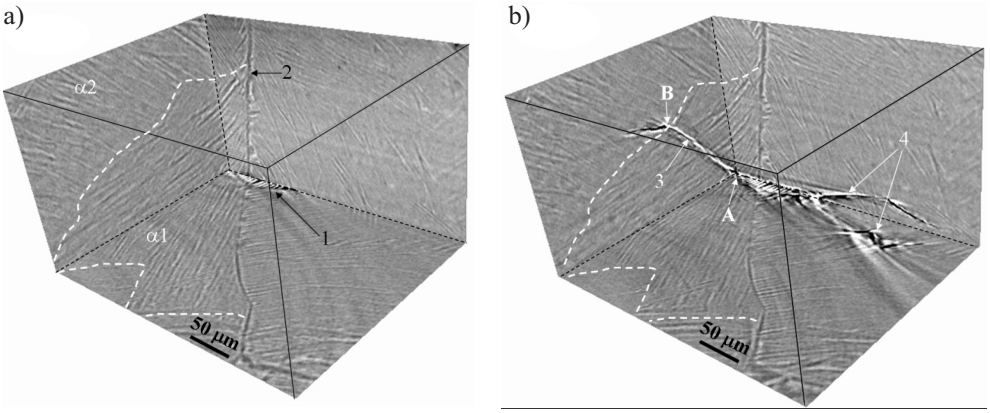

Fig. 4. 3D reconstructed images in three principal directions of titanium alloy sample: a) virgin state; b) after 29000 cycles of fatigue test. 1 – notch at sample surface, 2 – β grain boundary, α1, α2 – two different lamellar colonies, 3, 4 – two different cracks, A – point where crack initiates, B – point where crack deflects

The phase contrast is particularly interesting to be generated when no attenuation contrast between two different materials or phases exists, such as between aluminum and silicon (Buffiere *et al.* 1999), or in the present case between α and β titanium phases. It is also a very powerful mean to detect unresolved cracks (i.e. cracks which present a width smaller than the spatial resolution). Moreover, the difference in refractive index between the different phases in titanium alloy and air gives rise to different intensity of the phase contrast: One can verify from Figure 4b that the supposed lower difference in refractive index between α and β phases results in a weaker phase contrast than the one between cracks and titanium (n~1 for air and n~2.2 for titanium).

The comparison between Figure 4a and Figure 4b reveals very useful information. One can see in Fig. 4b that one crack (detail 3) has propagated fairly linearly within a colony (detail α1) between points A and B, then deviated at a boundary with a neighboring colony (detail α2). The computation of an oblique slice in the crack plane also reveals more interesting features of the crack development in interaction with the microstructure: sinusoidal shape of the crack front (between points B and C in Fig. 5a) and apparently crack branches propagating between lamellae (points 3a to 3d in Fig. 5a). The 3D rendering of this crack is displayed on Figure 5b with isosurfaces of the notch and β grain boundary. The figure also shows the isosurface of the intense phase contrast fringes generated by the unresolved

cracks (detail 5). The different features have been segmented using the region growth procedure. This alternative segmentation method to classical thresholding, constructs regions by starting from some user-provided voxels called seeds. Each seed grows and produces different 3D region. The progression is controlled by selecting a grey level interval surrounding the intensity value of the seed. More details about the algorithm can be found in (Nikolaidis *et al.* 2001). It is worth noticing that the difficult segmentation of the β grain boundary has bee facilitated once again by the white fringes which contain the region growing within the boundary. Figure 5b confirms the observations seen in the other figures. It also highlights that the crack "4" hardly propagates through the β grain boundary.

The images presented in this example show for the first time evidence of interaction between crack and microstructure in 3D. Indeed, the visualization of the deflection of the crack crossing over the boundary between two lamellar colonies is hardly achievable with standard 2D microscopic means. The detection of the branches is even more complex because the probability to visualize such event at the polished surface of a sample is small.

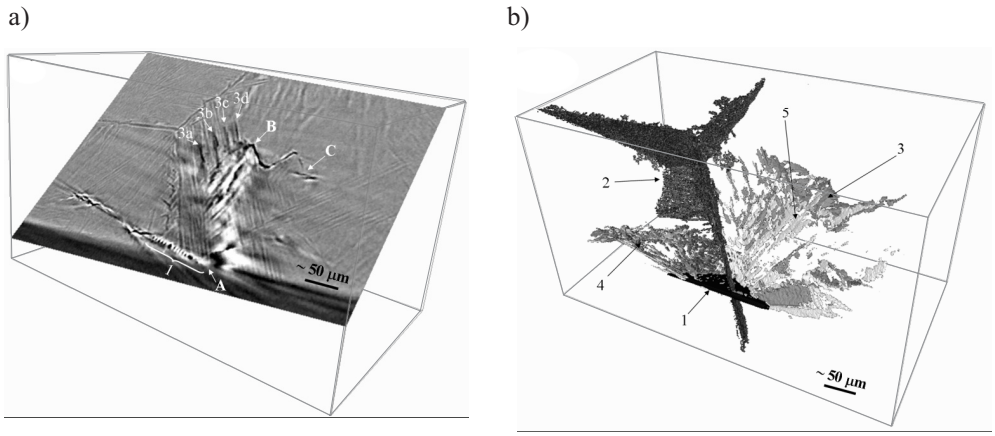

Fig. 5. Oblique slice- 29K cycles(a); 3D rendering of crack (b). 1 – notch, 2 – β grain boundary (dark grey), 3, 4 – two different cracks (grey), 3a, 3d – possible branches of crack (3), 5 – phase contrast corresponding to unresolved crack (light grey)

4. Conclusion

The present paper has shown, thanks to two different examples on effect of thermal oxidation of nuclear graphite and fatigue testing of titanium alloy, the wide capability of X-ray tomography imaging. The non-destructiveness and three dimensional images have proven to provide unique information that are not accessible using conventional 2D microscopy techniques. The maximum spatial resolution available at the present time is 0.3µm. However, researchers are currently working on improving systems to reach a spatial resolution up to 50 nm without sample size limitation, which will guarantee a serious alternative to electronic microscopy and give rise to new research avenues at the nanoscale.

References

[1] Babout L., Marrow T.J., Mummery P.M., Withers P.J.: *Mapping the evolution of density in 3D of thermally oxidised graphite for nuclear applications.* Scripta Mater., 54, (5), 2006, 829–834

[2] Babout L., Mummery P.M., Marrow T.J., Tzelepi A., Withers P.J.: *The effect of thermal oxidation on polycrystalline graphite studied by X-ray tomography.* Carbon, 43, 2005, 765–774

[3] Boller E.: *ID19 beamline webpage, ESRF*. URL. http://www.esrf.fr/UsersAndScience/Experiments/Imaging/ID19/. Last Update: 20/07/2005

[4] Buffiere J.-Y., Maire E., Cloetens P., Lormand G., Fougeres R.: *Characterization of internal damage in a MMC_p using X-ray synchrotron phase contrast microtomography.* Acta Materialia, 47, (5), 1999, 1613–1625

[5] Cloetens P., Pateyron-Salome M., Buffiere J.Y., Peix G., Baruchel J., Peyrin F., Schlenker M.: *Observation of microstructure and damage in materials by phase sensitive radiography and tomography.* Journal of Applied Physics, 81, 1997, 5878–5886

[6] Feldkamp L.A., Davis L.C., Kress J.W.: *Practical cone-beam algorithm.* Journal of Optical Society of America A, 1, (6), 1984, 612–619

[7] Lutjering G.: *Influence of processing on microstructure and mechanical properties of (α+β) titanium alloys.* Materials Science and Engineering A, 243, (1–2), 1998, 32–45

[8] Nikolaidis N., Pita I.: *3-D Image Processing Algorithms.* Wiley-Interscience, New York, 2001

[9] Russ G.C.: *The imaging processing handbook.* CRC Press, Boca Raton, 1995